

Modeling, analysis and simulation of "AC inductor" based converters

Ilya Zeltser, *Student Member, IEEE* and Sam Ben-Yaakov, *Member, IEEE*

Power Electronics Laboratory
Department of Electrical and Computer Engineering
Ben-Gurion University of the Negev
P.O. Box 653, Beer-Sheva 84105, ISRAEL.
Phone: +972-8-646-1561; Fax: +972-8-647-2949;
Emails: ilyaz@ee.bgu.ac.il, sby@ee.bgu.ac.il; Website: www.ee.bgu.ac.il/~pel

Abstract-The operation of converters that include power inductors with no DC current – defined here as "AC inductors" – was studied analytically, by simulation and experimentally. A SPICE compatible model was developed and the simulation results for small and large signal response were verified against theoretical and experimental results.

The behavior of the "AC inductor" based converters, as revealed in this study was compared to conventional PWM converter in which the power inductor is exposed to DC current ("DC inductor").

Based on the results of this study one can conclude that "AC inductor" based topologies are optimal for current sourcing applications, such as battery chargers, where differences between the average input and output voltages are expected to exist and develop over time. The advantage of these topologies in DC-DC converters, from the dynamics point of view, is that the control small signal transfer function (frequency perturbation to output voltage) is of first order for the practical bandwidth of operation.

I. INTRODUCTION

The classical method, utilized in most PWM converters, is to expose the power inductor to a DC current. Such inductors are referred to here as "DC inductors". In contrast, power conversion inductors that operate with zero average current are denoted "AC inductors". This latter operational method is similar to resonant load converters [1, 2] but in the topologies studied in this paper, a resonant capacitor is not applied [3, 4] and the current waveforms are non-sinusoidal [3-5]. The reason for the interest in "AC inductor" based topologies is the fact that they achieve soft switching [2, 3, 6-8]. The objective of this study was to analyze the behavior of the "AC inductor" based converters, to derive the analytical expressions for the large and small signal responses, to develop a behavioral SPICE compatible model for them, to evaluate the requirements of the control loop design and compensation networks for these systems and to compare their behavior to "DC inductor" based converters. This paper does not address the issues of losses or cost since the focus is here on the functional and control aspects only which have not been studied hitherto. The general aspects of the "AC inductor" based topologies can be found in earlier publications [e.g. 2-8].

II. LARGE SIGNAL ANALYSIS OF THE "AC INDUCTOR" BASED CHARGERS

To describe the behavior of AC inductor topologies, we first consider the non-isolated charger shown in Fig. 1. Isolation can be obtained by placing a transformer before the diode bridge. It is assumed that the exemplary full-bridge inverter operates with 50% duty cycle and hence generates a symmetrical bipolar square wave signal at its output. In this case, the voltages applied to both terminals of the inductor in Fig. 1 are bipolar and the inductor's current flows in both directions (Fig. 2) with zero average component. In the ideal case, the voltages seen by each inductor's terminals do not include DC components. In practical AC inductor circuits, due to non-symmetry of the inverter's output voltage, a DC component may appear at the left terminal of the AC inductor (Fig. 1). This error component can be removed by a series capacitor, or by applying peak current control.

During the time interval t_1 - t_2 (Fig. 2) the peak inductor current I_{pk} is:

$$I_{pk} = \frac{V_{bus} - V_{out}}{L} (t_2 - t_1) \quad (1)$$

where L is the inductance of the inductor. Similarly, during the time interval t_2 - t_3 I_{pk} is expressed as:

$$I_{pk} = \frac{V_{bus} + V_{out}}{L} (t_3 - t_2) \quad (2)$$

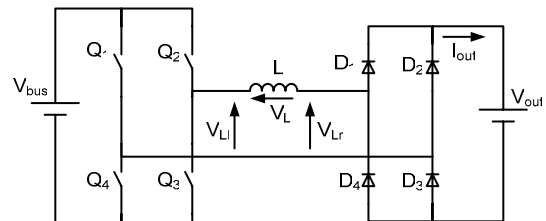


Fig. 1. Non-isolated full bridge battery charger with AC inductor.

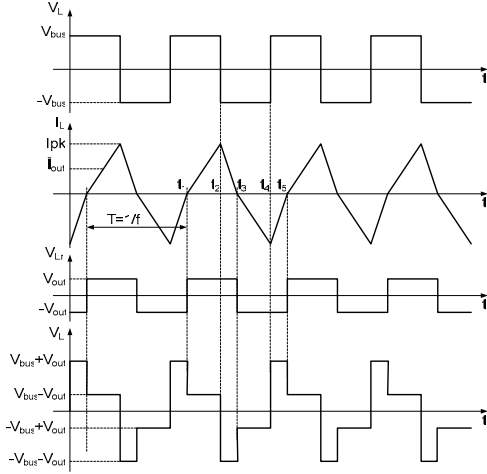


Fig. 2. Basic waveforms of the full bridge "AC inductor" based converter. From top to bottom: V_{L1} , Inductor current, V_{Lr} , voltage across inductor.

From (1) and (2), taking into account that (t_3-t_1) is half a switching cycle, yields:

$$(t_2 - t_1) + (t_3 - t_2) = I_{pk} L \frac{2V_{bus}}{V_{bus}^2 - V_{out}^2} = \frac{1}{2F} \quad (3)$$

where F is the switching frequency. Rearranging (3) back for I_{pk} we get:

$$I_{pk} = \frac{V_{bus}^2 - V_{out}^2}{4LFV_{bus}} \quad (4)$$

The output current is the rectified inductor's current as depicted in Fig. 3. Since the output current is of triangular shape, its average value is half its peak value:

$$\bar{I}_{out} = \frac{1}{2} I_{pk} = \frac{V_{bus}^2 - V_{out}^2}{8LFV_{bus}} \quad (5)$$

where \bar{I}_{out} is the output current averaged over the switching cycle. The average power delivered to the output is thus:

$$P_{out} = \bar{I}_{out} \cdot V_{out} \quad (6)$$

Substituting (5) into (6) yields:

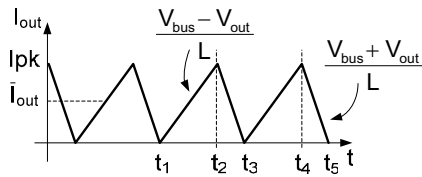


Fig. 3. Output current of an "AC inductor" based converter.

$$P_{out} = \frac{V_{out}}{8LF} \frac{V_{bus}^2 - V_{out}^2}{V_{bus}} \quad (7)$$

To develop the behavioral average model of the "AC inductor" we will focus on the average value of the output current which is the rectified inductor's current, while taking into account that the average current through the main inductor is zero. During the time period t_1-t_2 (Fig. 3) the voltage applied to the inductor is $(V_{bus}-V_{out})$ whereas during t_2-t_3 it is $-(V_{bus}+V_{out})$. Since $(t_2-t_1)+(t_3-t_2)=1/2F$ the average voltage applied to the inductor can be expressed as:

$$\bar{V}_L = (V_{bus} - V_{out}) \cdot (t_2 - t_1) \cdot 2F - (V_{bus} + V_{out}) \cdot (t_3 - t_2) \cdot 2F \quad (8)$$

Equation (8) can be represented by the schematic diagram shown in Fig. 4.

Equating (1) and (2), we will find the ratio between the two time periods:

$$\frac{t_3 - t_2}{t_2 - t_1} = \frac{V_{bus} - V_{out}}{V_{bus} + V_{out}} \quad (9)$$

Expressing (t_3-t_2) as $\frac{1}{2F} - (t_2 - t_1)$ and substituting into (9), the time period (t_2-t_1) is found as follows:

$$(t_2 - t_1) = \frac{V_{bus} + V_{out}}{4V_{bus}F} \quad (10)$$

Considering (10), the expression for the left voltage source of Fig. 4 is reduced to $\frac{V_{bus}^2 - V_{out}^2}{2V_{bus}}$.

That is, the magnitude of the left voltage source is determined by input and output voltages. The right voltage source can be set to be a function of the output current and the switching frequency by applying (2).

From (2) the time period (t_3-t_2) duration is given as:

$$(t_3 - t_2) = \frac{LI_{pk}}{V_{bus} + V_{out}} \quad (11)$$

Since the current is of a triangular shape (Fig. 3), the peak is twice its average value and hence:

$$(t_3 - t_2) = \frac{2L\bar{I}_{out}}{V_{bus} + V_{out}} \quad (12)$$

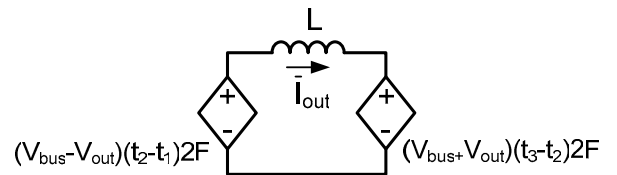


Fig. 4. Schematic diagram of equation (8).

Applying (12) to the right voltage source of Fig. 4, the expression is rewritten as $4L\bar{I}_{out}F$.

The resulted average model is shown in Fig. 5.

III. SMALL SIGNAL ANALYSIS OF THE "AC INDUCTOR" BASED CHARGER

The behavioral model of Fig. 5 was further used to obtain the ac response of the "AC inductor" based systems.

A. Small signal current response to a disturbance in the input voltage.

We assume that the circuit operates at a given input voltage V_{bus} , output voltage V_{out} and frequency F . The dependence of the inductor's current changes i_L on a small signal disturbance in input voltage V_{in} (v_{in}), was found by linearizing the two dependent sources of Fig. 4 and assuming that all variables except the input voltage are constant:

$$\bar{i}_{out} = \frac{\frac{1}{2} \left(1 + \frac{V_{out}^2}{V_{bus}^2} \right) v_{in} - 4FL\bar{I}_{out}}{sL} \quad (13)$$

Taking into account the triangular shape of the inductor's current, that is $\bar{i}_{out} = i_{out} / 2$ and rearranging:

$$\frac{i_{out}}{v_{in}} = \frac{K_1}{s + 4F} \quad (14)$$

$$\text{where } K_1 = \frac{V_{bus}^2 + V_{out}^2}{V_{bus}^2 L}.$$

B. Small signal current response to a disturbance at the output voltage.

Following the same procedure as above but for the disturbance in the output voltage v_{out} , we find:

$$\frac{i_{out}}{v_{out}} = \frac{K_2}{s + 4F} \quad (15)$$

$$\text{where } K_2 = -\frac{2V_{out}}{V_{bus}L}.$$

Equations (14) and (15) imply that the output current response is determined by the switching frequency F and that the disturbance frequency has little effect. That is, the small signal current in the inductor (even at low perturbation frequencies) will be limited by the inductor's impedance at the switching frequency rather than by the low frequency impedance or the parasitic resistances.

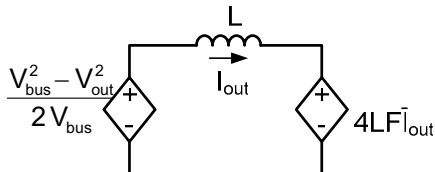


Fig. 5. Average large signal model of "AC inductor" based charger.

C. Inductor's current response to a modulating frequency.

In an electronic charger it is usually desirable to maintain a constant load current. One possible way to achieve that will be to control the switching frequency. That is, the control transfer function required for the design of the compensation network, is the response of the inductor's current to a modulation f in the switching frequency of the square-wave input voltage. To find this transfer function, the dependent sources of Fig. 5 were linearized assuming that the disturbance was in the switching frequency (Fig. 6). All the voltage sources were assumed to be constant. The small signal output current was found to be:

$$\bar{i}_{out} = -\frac{(4L\bar{I}_{out}f + 4L\bar{I}_{out}F)}{sL} \quad (16)$$

Substituting again that $\bar{i}_{out} = i_{out} / 2$ and rearranging:

$$\frac{i_{out}}{f} = -\frac{8P_{out}}{V_{out}} \frac{1}{s + 4F} \quad (17)$$

A typical transfer function of (17) plotted for $V_{bus}=100V$, $V_{out}=50V$, $P_{out}=100W$, and $F=62.5kHz$ is shown in Fig. 7.

The last equation implies that for low frequencies the inductor behaves as a resistor (flat response in Fig. 7). That is, even for a very slow disturbance in the switching frequency (very slow modulation of F) the changes in the inductor's current will be negligible for practical switching frequencies (tens of kilohertz). It follows that the AC inductor charger can be operated in open loop. This is a corollary of the fact that the AC inductor based converters behave as a current sources.

IV. THE "AC INDUCTOR" BASED DC-DC CONVERTER

In the general case of a DC-DC converter (rather than a battery charger), one cannot assume a constant output voltage. An example of DC-DC converter that applies an AC inductor is given in Fig. 8. Here the voltage source V_{out} of Fig. 1 is replaced by a resistive load in parallel with an output capacitor. The average model of this system is presented in Fig. 9. The output voltage in an AC inductor based DC-DC converter is regulated by modulating the switching frequency. Consequently, modulating-frequency to output-voltage transfer function is required for the control loop compensation design. This transfer function was derived by linearizing the model of Fig. 9.

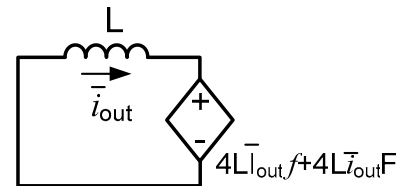


Fig. 6. Linearized average small signal model of AC inductor for small-signal injection in F (f).

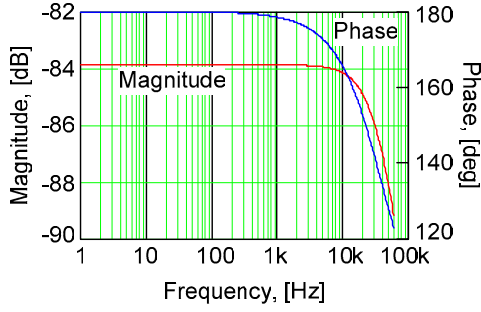


Fig. 7. Small signal response of the output current to a modulation in the switching frequency of the charger of Fig. 1.

It was assumed that the disturbance was in the switching frequency and the input voltage (V_{bus}) was constant. The resulting linearized model is presented in Fig. 10

Applying KVL to the left part of Fig. 10 yields:

$$-\frac{V_{out}}{V_{bus}} \bar{v}_{out} + sL\bar{i}_{out} + 4L(F\bar{i}_{out} + \bar{i}_{out}f) = 0 \quad (18)$$

From the right side circuitry of Fig. 10, the small signal average inductor current (\bar{i}_{out}) can be found as:

$$\bar{i}_{out} = \bar{v}_{out} \frac{1 + sC_{out}R_{out}}{R_{out}} \quad (19)$$

Substituting it back into (18) yields:

$$\frac{v_o}{f} = -\frac{4V_{out}\tau_L}{\frac{s^2}{w_0^2} + s\left(\frac{4F}{w_0^2} + \tau_L\right) + (4F\tau_L + k)} \quad (20)$$

$$\text{where } w_0 = \frac{1}{\sqrt{L \cdot C_{out}}}, \tau_L = \frac{L}{R_{out}}, k = \frac{V_{out}}{V_{bus}} \quad (21)$$

The poles of this transfer function are located at:

$$f_{1,2} = \frac{1}{4\pi} \left[\left(4F + w_0^2\tau_L \right) \pm \sqrt{\left(4F + w_0^2\tau_L \right)^2 - 4w_0^2(4F\tau_L + k)} \right] \quad (22)$$

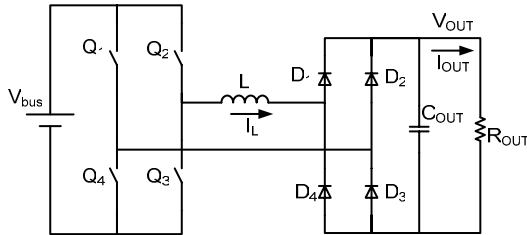


Fig. 8. DC-DC converter with AC inductor.

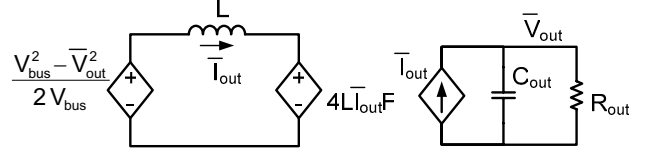


Fig. 9. Average model of a DC-DC converter with "AC inductor".

By dividing and multiplying expression (22) by F it can be converted to the form:

$$f_{1,2} = \frac{F}{4\pi} \left[\left(4 + \frac{w_0^2\tau_L}{F} \right) \pm \sqrt{\left(4 - \frac{w_0^2\tau_L}{F} \right)^2 + \frac{4w_0^2k}{F^2}} \right] \quad (23)$$

Equation (23) reveals that the radicand is positive, so the system has two real poles.

Equation (23) can also be rewritten as follows:

$$f_{1,2} = \frac{F}{4\pi} \left[\left(4 + \frac{w_0^2\tau_L}{F} \right) \pm \left(4 - \frac{w_0^2\tau_L}{F} \right) \sqrt{1 + \frac{\frac{4w_0^2k}{F^2}}{\left(4 - \frac{w_0^2\tau_L}{F} \right)^2}} \right] \quad (24)$$

It can be shown (Appendix A) that in practical applications the right term of the radicand is much smaller than unity. Hence, the square root in (24) can be expanded into the Taylor series (omitting all the terms above the second one):

$$\sqrt{1 + \frac{\frac{4w_0^2k}{F^2}}{4 - \frac{w_0^2\tau_L}{F}}} \approx 1 + \frac{1}{2} \frac{\frac{4w_0^2k}{F^2}}{4 - \frac{w_0^2\tau_L}{F}} \quad (25)$$

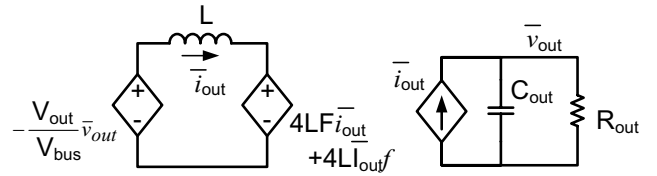


Fig. 10. Average model of Fig. 9 linearized for the disturbance in switching frequency.

Substituting (25), into (24) we can approximate the poles of (20) as:

$$f_1 \approx \frac{F}{2\pi} \left[\frac{w_0^2 \tau_L}{F} + \frac{\frac{w_0^2 k}{F^2}}{4 - \frac{w_0^2 \tau_L}{F}} \right] \quad (26)$$

$$\text{and } f_2 \approx \frac{2}{\pi} F \left[1 + \frac{1}{4} \frac{\frac{w_0^2 k}{F^2}}{4 - \frac{w_0^2 \tau_L}{F}} \right]$$

Since the average methodology used to derive the transfer function (20) can only be applied up to the half the switching frequency ($F/2$), the pole f_2 , that is apparently higher than ($F/2$), will not be taken into consideration.

The term $\frac{w_0^2 \tau_L}{F}$ in (26) can be related to the output ripple as follows.

Let's assume that the peak-to-peak output voltage ripple is kept within R_{pl} , defined as:

$$R_{pl} = \frac{\Delta V_{out}}{V_{out}} \quad (25)$$

where ΔV_{out} is the output voltage peak-to-peak deviation given as:

$$\Delta V_{out} = \frac{Q}{C_{out}} = \frac{1}{C_{out}} \frac{\bar{I}_{out}}{8F} \quad (26)$$

where Q is the charge transferred to the output capacitor during the output switching cycle.

Expressing \bar{I}_{out} as $\frac{V_{out}}{R_{out}}$ and substituting (21) yields:

$$\frac{\Delta V_{out}}{V_{out}} = \frac{w_0^2 \tau_L}{8F} \quad (27)$$

Applying (25) we find:

$$\frac{w_0^2 \tau_L}{F} = 8 \cdot R_{pl} \quad (28)$$

In modern power conversion systems, the output ripple is normally kept very low (1% or less) and consequently $8 \cdot R_{pl}$ is much smaller than 4. So the expression for f_1 , (26), can be rewritten as follows:

$$f_1 \approx \frac{F}{2\pi} \left[\frac{w_0^2 \tau_L}{F} + \frac{w_0^2 k}{4F^2} \right] = \frac{w_0^2 \tau_L}{2\pi} + \frac{w_0^2 k}{8\pi F} \quad (29)$$

Finally, substituting (21), using (5) and expressing \bar{I}_{out} as $\frac{V_{out}}{R_{out}}$ yields:

$$f_1 \approx \frac{1}{2\pi C_{out} R_{out}} \frac{1+k^2}{1-k^2} \quad (30)$$

The implication of (30) is that, similar to the charger discussed above, the generic behavior of the AC Inductor based DC-DC converter is that of a current source and hence the dynamics is primarily controlled by the output filter pole. However, the pole location of the system is modified by a term that is a function of the dc transfer ratio of the system (k). For small values of k the pole shift will be small but for larger k values the shift is significant (e.g. for $k=0.8$ the location of the basic $R_{out}C_{out}$ pole will be shifted by a factor of 4.5). This, of course, has to be taken into account when designing a controller for AC inductor based DC-DC converters.

The reason for the pole shift may have to do with the fact that a larger k implies a smaller amplitude of the voltage pulses across the inductor, which is somehow reducing its current sourcing capabilities. Further study is evidently required to clear up this point. Fig. 11 represents a typical response of (20) plotted for $V_{bus}=100V$, $V_{out}=50V$, $L_{in}=75\mu H$, $F=62.5kHz$, $C_{out}=220\mu F$ and $R_{out}=25\Omega$ ($k=0.5$, $\tau_L=3\mu s$, $w_o=7.8kHz$). The pole f_1 in this case is located at 48Hz. This small signal response can also be obtained by running an AC analysis on the SPICE compatible model of Fig. 9.

V. EXPERIMENTAL AND SIMULATION RESULTS

The analytically derived small signal response of the AC inductor DC-DC converter was verified by running a full circuit (cycle-by-cycle) simulation. The dots on the Bode diagram of Fig. 11 show the results of cycle-by-cycle simulation for the same parameters used in the analytical calculation (continuous line). Small signal (AC) SPICE simulation carried out on the average large-signal model of Fig. 9 produced results which were identical to the analytically based plots.

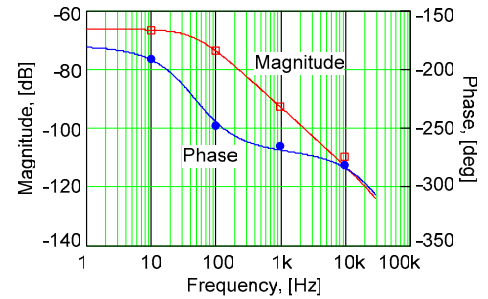


Fig. 11. Small signal response of the output voltage to a modulation in the switching frequency of an "AC inductor" based DC-DC converter. Continuous plot: analytical and average simulation results. Dots: full (cycle by cycle) simulation.

The "AC inductor" based charger was tested experimentally using a half bridge topology with a blocking capacitor (Fig.12). The battery load was modeled in the experimental setup by an RC network with very large time constant so it can be considered practically zero impedance at the tested small signal frequencies. The inductor was $75\mu\text{H}$, load capacitor $4700\mu\text{F}$, and load resistor 25Ω . DC blocking capacitor was (1.5mF) . The bus voltage was 100VDC . Output voltage was about 50VDC . The switching frequency was set to 62.5kHz and power transferred to the load was about 100W .

Fig. 13 shows the response of the output current to the disturbance at the output voltage. The output voltage was modulated by adding a 50Hz ac voltage source in series with the RC network. The injected signal had an amplitude of $10\text{V}_{\text{pk-pk}}$. This resulted (Fig. 13) in an envelope amplitude of the inductor current of about $0.55\text{A}_{\text{pk-pk}}$. By setting f to 50Hz , v_{out} to 10V in (15) we get the value of 0.54A which is in good agreement with the measured value.

Output current response to a modulated switching frequency is presented in Fig. 14. The frequency was modulated by a 1kHz sinusoidal modulating signal. Maximum frequency deviation was 10kHz (modulation index of 10). The measured current to frequency ratio was about $66[\mu\text{A}/\text{Hz}]$. The ratio calculated from (17) is $64[\mu\text{A}/\text{Hz}]$.

An expanded view of the output current, modulating signal as well as the voltage across the inductor is shown in Fig. 15.

VI. COMPARISON TO "DC INDUCTOR" BASED TOPOLOGIES

In the Buck type battery charger of Fig. 16, the output current cannot be controlled by duty cycle alone and hence in a practical design will entail an inner current loop. This is in contrast to the "AC Inductor" based topology (Fig. 1) that can be operated in open loop since the output current can be conveniently controlled by the switching frequency (Eq. 5). Another advantage of the "AC inductor" system is the ability to isolate the output from the input by a transformer placed before or after the AC inductor.

Similar to the case of the "AC inductor" the small signal response of the "DC Inductor" based converter is also of second order but unlike the case of the "AC inductor" converter, the system normally includes two complex poles.

VII. DISCUSSION AND CONCLUSIONS

This study introduces a behavioral SPICE compatible model for "AC inductor" based power converters. The model was applied to analyze the large and small signal responses of an "AC inductor" electronic charger and a DC-DC converter.

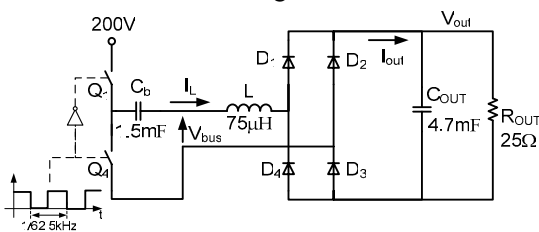


Fig. 12. Experimental setup.

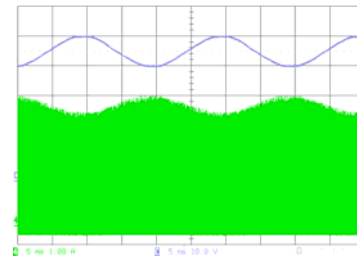


Fig. 13. Output current response to an output voltage modulation. Upper trace: Modulating voltage $10\text{V}/\text{div}$; Lower trace: Output current $1\text{A}/\text{div}$; Horizontal scale: $5\text{ms}/\text{div}$.

The analytical expressions derived by proposed model were further used to compare the large and small signal behavior of "AC" and "DC inductor" based power converters. The analytical derivations and simulations of this study were verified experimentally. Good agreement was found between simulation and experimental results.

The results of the analysis show that the "AC inductors" chargers behave as a current source due to the large impedance of the "AC inductor". Hence, these chargers have a high immunity to average voltage disturbances at either input or output side. As a result, they can be operated as current sources in open loop configuration without the need for current feedback. On the other hand, a "DC inductor" based charger behaves as a voltage source and hence a small difference between the average voltages of the inductor's terminals may cause current run-away and therefore, a tight current feedback loop must be applied.

The analysis further revealed that for AC inductor based DC-DC converters, the small signal response of the output voltage to a modulation of the switching frequency is of second order. It was further found that in practical designs, this transfer function has real pole. This implies that for a practical control loop bandwidth, the relevant portion of the transfer function is "well behaved" and the control loop can be compensated using a simple compensation networks, such as lag-lead, with no need for a second inner loop feedback. This is in contrast to the case of the "DC inductor" based converter (say Buck) which typically follows the behavior of a second order system with complex pole.

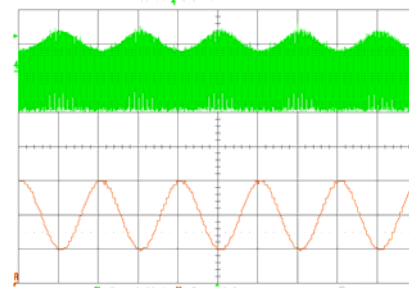


Fig. 14. Output current response to a modulation of the switching frequency. Upper trace: Output current $2\text{A}/\text{div}$; Lower trace: Modulating frequency $10\text{kHz}/\text{div}$; Horizontal scale: $0.5\text{ms}/\text{div}$.

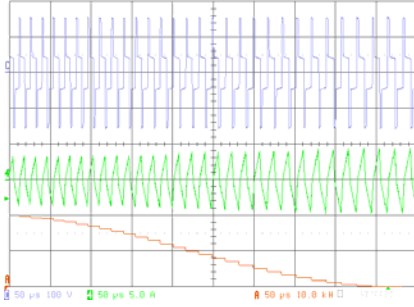


Fig. 15. Expanded view of AC inductor's key waveforms. Upper trace: Inductor's voltage 100V/div. Middle Trace: Inductor's current 5A/div. Lower Trace: Switching frequency 10kHz/div (carrier frequency 62.5kHz). Horizontal scale: 50us/div

The lower order response of the "AC inductor" converter simplifies and reduces the cost of the control circuitry especially if digital control is preferred.

Based on the results presented in this study one can conclude that "AC inductor" based topologies are optimal for current sourcing applications, such as battery chargers and electronic ballasts where differences between the average input and output voltages are expected to exist or develop over time. In DC-DC converter cases, the advantage of the AC inductor based converters is the more convenient small signal response. These benefits are additional to the soft switching feature which would be probably the main reason for choosing these topologies. The disadvantage (from the dynamics point of view) is the higher output impedance, similar to the case of a DC inductor converter with an inner current loop.

APPENDIX A

JUSTIFYING THE APPROXIMATION USED IN PAPER

It is shown below that the term $\frac{4w_0^2k}{F^2}$ is small as

compared to $\left(4 - \frac{w_0^2\tau L}{F}\right)^2$, i.e.:

$$\frac{4w_0^2k}{F^2} < \left(4 - \frac{w_0^2\tau L}{F}\right)^2 \quad (A1)$$

It is evident that the both sides of the equation (A1) are positive and hence it can be reduced to:

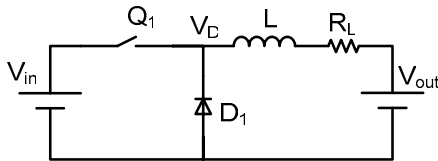


Fig. 16. Buck type battery charger with "DC inductor".

$$\frac{2w_0\sqrt{k}}{F} < 4 - \frac{w_0^2\tau L}{F} \quad (A2)$$

After rearranging we get:

$$2\sqrt{k} \frac{w_0}{F} + \frac{w_0^2\tau L}{F} < 4 \quad (A3)$$

k is the ratio of the output to input voltage which is always less than unity. Hence, the upper limit of \sqrt{k} is unity as well. The resonant frequency of the input inductor and output capacitor (w_0) will be chosen in practical applications well below the switching frequency in order to reduce the output current's ripple, so the ratio $\frac{w_0}{F}$ is very small. The second term of the left side of (A3) is also very small in practical applications as explained above (see section III, eq. (28)). Consequently, in practical designs the condition (A3) would be easily met.

For the system presented in section III ($k=0.5$, $\tau_L=3\mu s$, $w_0=7.8kHz$, $F=62.5kHz$), the left side of (A1) is equal to 0.031 whereas its right side is 15.977.

ACKNOWLEDGMENT

This research was supported by THE ISRAEL SCIENCE FOUNDATION (grant No. 113/02) and by the Paul Ivanier Center for Robotics and Production management.

REFERENCES

- [1] R. W. Erickson, "Resonant Conversion," chap. 19 in *Fundamentals of Power Electronics*, Chapman&Hall, N.Y., 1997.
- [2] S. Sato, S. Moisseev, and M. Nakaoka, "A novel synchronous rectifiers based ZVS-PWM DC-DC power converter with extended soft-switching operational range," *IEEE The 25th International Telecommunications Energy Conference, INTELEC'03*, pp. 268-273, 19-23 October 2003.
- [3] I. D. Jitaru, "A 3 kW soft switching DC-DC converter," *IEEE Fifteenth Annual Applied Power Electronics Conference and Exposition, APEC 2000*, vol. 1, pp. 86 - 92, 6-10 Feb. 2000.
- [4] Y. Zhang, P. C. Sen, "A new ZVS phase-shifted PWM DC-DC converter with push-pull type synchronous rectifier," *IEEE Canadian Conference on Electrical and Computer Engineering, CCECE 2003*, vol. 1, pp. 395-398, 4-7 May 2003.
- [5] F. Krismer, J. Biela, and J. W. Kolar, "A Comparative Evaluation of Isolated Bi-directional DC/DC Converters with Wide Input and Output Voltage Range," *IEEE Industry Applications Conference, Fourteenth IAS Annual Meeting, vol. 1*, pp. 599 - 606, 2-6 October 2005.
- [6] C. Hang-Seok, J.H. Lee, B. H. Cho, J. W. Kim, "Analysis and design considerations of zero-voltage and zero-current-switching (ZVZCS) full-bridge PWM converters," *IEEE 33rd Annual Power Electronics Specialists Conference, PESC 2002*, vol. 4, pp. 1835-1840, 23-27 June 2002.
- [7] M. Xu, Y. Ren, J. Zhou, and F. C. Lee, "1-MHz Self-Driven ZVS Full-Bridge Converter for 48V Power Pod and DC/DC Brick," *IEEE Transaction on Power Electronics*, vol. 20, pp. 997-1006, 2005.
- [8] S. TingTing, H. Nianci, "A novel zero-voltage and zero-current-switching full-bridge PWM converter," *Eighteenth Annual Applied Power Electronics Conference, APEC 2003*, vol. 2, pp. 1088-1092, 2003.
- [9] S. Ben-Yaakov, "Average simulation of PWM converters by direct implementation of behavioral relationships," *International Journal of Electronics*, vol. 77, pp. 731-746, 1994.